Compositional and microstructural characterization of Celtic silver coins from northern Italy using neutron diffraction analysis

(Article begins on next page)

15 October 2023

Compositional and microstructural characterization of Celtic silver coins from northern Italy using neutron diffraction analysis.

J. Corsi,[a] F. Grazzi,[b] A. Lo Giudice,[a] A. Re,[a] A. Scherillo,[c] D. Angelici,[a] S. Allegretti,[a] and F. Barello[d]

[a] Dipartimento di Fisica, Università di Torino and INFN, Sezione di Torino, Via P. Giuria 1, 10125 Torino, Italy.

[b] ISC-CNR, Via Madonna del Piano 10, 50019 Sesto Fiorentino (FI), Italy.

[c] Rutherford Appleton Laboratory (ISIS Facility), Chilton, Didcot, Oxon OX11 0QX, United Kingdom and IPCF-CNR, Viale F. Stagno D'Alcontres 37, Messina (ME), Italy

[d] Soprintendenza Archeologia del Piemonte, Piazza S. Giovanni 2, 10122 Torino, Italy.

The silver coinage of Celtic tribes settled in northern Italy (IV-I century B.C.) is a topic characterized by several issues, such as chronology, attributions and relationships between emissions produced in different periods. In order to provide numismatists with new data, several specimens, belonging to different typologies, have been analysed with neutron diffraction technique to overcome surface alteration and to provide bulky compositional and structural information of the coins. Measurements performed with the INES diffractometer at the ISIS facility provided essential data for numismatics research. A clear silver debasement occurring between the first and latter emissions has been traced, due to inflation processes which can be related with the increasing power of Roman Republic in the Cisalpine region. Moreover, compositional data enabled for the first time to identify internal evolutions inside typologies defined by numismatists. The silver loss has also been used to establish a relative chronology between different emissions. Other parameters such as texture index, residual strains and grain dimensions have been useful to understand technical aspects of minting procedures during Iron Age.

Introduction

The importance of physico-chemical material characterization in studies on the Celtic silver coinage from northern Italy has been rarely considered. Unlike Greek and Roman coins, which have been analysed with several approaches to answer different historical issues, Celtic coins from this area still lack of reliable scientific data. Indeed, the few published compositional information[1] have been carried out on untreated coins with X-ray fluorescence (XRF) technique. However, silver-copper alloy coins, especially those with a fineness < 80 wt. % of silver, have actually been demonstrated to be heavily affected by thick silver-surface-enriched layers (up to 200 µm), so data obtained on un-sectioned samples by means of surface techniques, including XRF or PIXE, are not reliable[2-4].

For this reason, a wide characterization project involving the use of neutron-based techniques has been developed. The first compositional results were obtained with Prompt Gamma Activation Analysis (PGAA) and have been recently published[5]. To increase the statistical sample and to investigate also microstructural properties, a bulk and non-destructive technique such as neutron diffraction (ND) has been used in this work for the characterization of a further selection of Celtic coins. Time-of-flight neutron diffraction (TOF-ND) measurements have been performed with the INES diffractometer at the ISIS facility on our specimens.

TOF-ND technique is a powerful tool for the analysis of metal, especially in archaeometric studies as precious archaeological artefacts can be analysed in air without any sampling or preparation[6,7]. This technique has been often applied for coins characterization in the last years[8-14], and results were very

promising for numismatics studies. TOF-ND analysis is able to provide both compositional and structural information. In particular, the possibility to extract information from diffraction patterns concerning texture index, residual strain and grain dimension, has been considered very useful.

This study had therefore a twofold aim. The first was to provide ratios of precious and base metal (silver and copper respectively), to verify whether a debasement was present among coins dated to different periods and to understand their exchange ratios with foreign currency (e.g. Roman and Massalian currency). The second was to bring new data for the understanding of minting procedures during Iron Age, being documentary evidence absent.

Historical background

The pre-Roman coinage from northern Italy, commonly defined as "Celtic coinage of the Po valley", collects different series of silver coins, produced by several tribes settled in a wide territory known in the subsequent Roman age as the Cisalpine Gaul. These tribes, either of Celtic or non-Celtic culture, minted their own coinage in a period which spans from the 4th up to the 1st century B.C., even if dating of the first emissions is still debated. They emitted mainly drachms, but some rare fractions (obols, diobols or hemidrachms) are known as well. The silver unit, the drachm, even of different tribes, is always characterized by the imitation of the iconography of Massalia's (present day Marseille, France) heavy drachm, depicting a lion with the ethnic abbreviation ΜΑΣΣΑ[ΛΙΗΤΩΝ] on reverse and the head of Artemis on the obverse. The reason for this peculiar iconographic choice probably lies in the deep relationships between the city founded by Greeks and the Celts, who were commonly hired by Massalia as mercenaries. The imitative emissions started soon after the minting of Massalia's prototypes and lasted for some centuries, until the Roman conquest of northern Italy (creation of Cisalpine Gaul's province around 89 B.C.) and the definitive introduction of Roman currency.

The study of this Iron Age coinage began only in the second half of XIX century. The first extensive work, by A. Pautasso[15], was published in 1966 and was based almost exclusively on a stylistic study of specimens kept in public and private collections and on the analysis of coins from hoards.

Conclusions by A. Pautasso have been over the last years partially revised, in the light of new findings and thanks to the developing of artefacts distribution maps and stratigraphic excavations. In the last two decades, E.A. Arslan proposed a new historical classification and attribution of these coins[16], based on the evidence of single finds. He developed a new cataloguing grid, suggesting attributions to different human groups (e.g. Cenomanes, Insubres, Libici, Veneti) and making hypotheses concerning the location of the ancient emission centers. He organized the Cisalpine coinage into 22 types of drachmas and 6 types of minor fractions.

Nevertheless, despite the richness of studies published in the last years, some scholars disagree with Arslan's research setting (e.g. M.H. Crawford[17] and G. Gorini[18]) and much work has still to be done in order to fully understand the coin production in Northern Italy during Iron age, both from an archaeological and a numismatics point of view.

Samples

This work is focused on the silver unit minted by Cisalpine Celts, the drachm. Results presented in this work are all related to silver drachmas produced in different periods and attributed to different tribes (Fig. 1). They mainly come from two hoards kept at the Museo di Antichità in Torino (Italy): the votive deposit from Serra Riccò (GE), currently consisting of 164 specimens, and the hoard of Biandrate (NO), with 40 coins. A third hoard is kept in the Museo Civico of Casale Monferrato, probably found in Balzola (AL) with 240 coins. Other specimens come from the historical collection of the Museo di Antichità of Torino and from the important Carlo Alberto's royal collection (Medagliere Reale) kept at the Armeria Reale in Torino. In these last cases the provenance has not been recorded.

The analysis has been performed on a selection of 33 specimens coming from all the above-mentioned hoards and collections. The coins selected for the analyses are reported in Table 1 along with their code and their weight. Nonetheless, being the classification non-shared among all the scholars, we will indicate for simplicity's sake the coins on the base of their main stylistic features. According to the shape of the lion, we can divide the Cisalpine coinage into the following main streams, all deriving from the Massalia's heavy drachm (Fig. 1a):

1. Massa α type (Fig. 1b). These rare drachmas are the first imitations, probably minted by local tribes settled in the surroundings of Massalia. Their average weight is the same of the official drachmas (~ 3.6 g). Dating is still controversial and the hypotheses span from 380 B.C. up to 215 B.C.
2. Massa β type (Fig. 1c). This not yet well defined group collects drachmas with a lighter weight (although recalling the heavy drachm) and different styles. They could be the first imitative coins produced in northern Italy.
3. Naturalistic-lion type (Fig. 1d). This type is present in the most ancient hoards in northern Italy and is often associated with the scorpion-lion type. The lion is depicted as natural. The average weight of these drachmas is 3.0 grams and they were produced in northern Italy.
4. Scorpion-lion type (Fig. 1e). Often associated with the previous type, is characterized by a lion which denotes a figurative Latenian culture. The lion has been described as similar to a scorpion. The average weight of these drachmas is 3.0 grams and they were produced in northern Italy during III century B.C., as the previous type.
5. Wolf-lion type (Fig. 1f). This type belongs to a second phase of the Cisalpine coinage, when the average weight decrease up to 2.6 grams. They were produced in northern Italy from the end of III century B.C. onwards.

[Fig.1]

Experimental

TOF-ND measurements have been carried out at the ISIS pulsed neutron source (Rutherford Appleton Laboratory, Chilton-Didcot, UK) using the INES TOF diffractometer of the Italian Neutron Experimental Station. INES is a multipurpose powder neutron diffractometer[19], often used for archaeometric applications[20]. It is characterized by an excellent resolution ($\Delta d/d = 0.1\%$) in the 0.1–2.1 Å range, granted by a long primary flight path from the moderator. The total d-spacing range extends up to 12 Å, providing a good coverage of the kinematical range and therefore allowing to study different types of materials. The instrument is equipped with 144 ^{3}He squashed detectors, grouped in 9 banks, covering a range of about 170° on the horizontal scattering plane. Each bank lies on a circle of 1 m radius from the diffractometer centre. The sample container is a large tank (80 cm diameter and about 0.5 m^3 volume) that allows the study of even large objects, including bulky archaeological artefacts. If necessary, the tank can operate in vacuum. On the tank is also placed a gamma ray detector for neutron resonance capture analysis (NRCA), which provides useful qualitative elemental data on the sample[21]. In addition, a neutron imaging system is available to check the sample position within the tank[22,23].

At ISIS, neutrons are produced by a spallation reaction, due to protons impinging onto a W target with a frequency of 50 Hz, and slowed-down by different types of moderators. The INES beamline makes use of an ambient-temperature water moderator; neutrons are then selected by a nimonic chopper to filter out high-energy neutrons and to let arrive at the sample position only those in the wavelength interval 0.17–3.24 Å.

The relation between the available interval of d-spacing and the neutron time-of-flight is the following:

$$d = \frac{2\,\pi}{Q} = \frac{h\,t}{2\,m\,L\,sin\theta}$$

where Q is the momentum transfer, h is the Planck's constant, t the arrival time of flight, L is the neutron total flight path, m is the neutron mass and θ is half of the scattering angle.

Measurements and data analysis

The coins under analysis were inserted in pockets made of vanadium to avoid undesirable Bragg peaks from sample holder and mounted on a 4 samples carousel inside the tank that was then evacuated to avoid scattering of neutrons by air (especially by hydrogen). Samples alignment with the beam was checked by means of the neutron camera and the beam size (maximum of 38 x 38 mm^2) was reduced at the dimension of the coin, thanks to motorized and remotely-controlled jaws placed between the shutter and the sample. This enabled to always get information from the entire volume of the objects considered in this work. Diffraction measurements lasted between 4 and 8 hours per coin, considering an average proton beam current of 160 μA/h.

The obtained diffraction patterns, according to Bragg's law, show several peaks whose positions are directly related to the crystal lattice dimensions of the different phases in the sample. These patterns plot intensities vs time of flight, which can be easily converted in wavelength, d-spacings or Q scales. Before any refinement, each pattern is normalized to the incoming white beam recorded by a monitor detector placed between the jaws and the sample.

In this work, the analysis of diffraction patterns has been carried out using the GSAS code[24] and the EXPGUI interface[25], to refine structural parameters and calculate phase weight fractions. The first step in the analysis of a multi-phase sample is the identification of each individual crystalline phase pattern. Association of measured peak positions with calculated or observed positions of pure single-phase fingerprints can be made using database search-match routines available online[26]. A Crystallographic Information File (*cif*) referred to a specific published characterization study of a certain material is usually downloaded and used as a reference for d-spacings. Once the phases are identified, a quantitative phase analysis through the Rietveld refinement[27] can take place. The phase analysis has been performed on data collected in the first 8 INES banks, where the main reflections are present and the resolution still enables them to be discriminated. The lattice parameters of major phases, instead, were determined on the first bank pattern, collected at high angles (at 2θ = 170.6 degrees), where the resolution is higher and offsets due to errors in the sample positioning can be considered negligible up to 6 mm.

In GSAS code, the instrumental parameters (e.g. DIFC, DIFA, ZERO) are stored in an Instrument Parameter File obtained from the refinement of a standard silicon (untextured powder 640c) diffraction pattern and are all listed and defined in the GSAS manual[24].

The profile function used to fit patterns is strictly correlated to the type of moderator used. In the case of the INES water moderator the diffraction peaks shape can be approximated by a pair of back-to-back exponentials and a pseudo-Voigt functions (in GSAS, TOF profile function 4).

At last, starting from d-spacing and phase composition obtained by means of GSAS code, the silver content, which is one of the most important information for numismatists, was calculated using the procedure described below. To check the results obtained with this method, a series of two standards (MBH) and one reference material (Goodfellow) has been analysed as well (see Table 1).

Results and discussion

Phase analysis of Celtic coins

The analysis of diffraction patterns of the 33 coins show peaks related to few phases only (Table 1). Two major phases have been observed: the copper-rich phase (α) and the silver-rich phase (β). This

result is not surprising since silver and copper have a very small solubility range and tend to give phase separation, as shown in the biphasic thermodynamic diagram[28]. Both have a FCC cell, and in the patterns we are able to see several peaks, the majors corresponding to the (111), (200), (220), (311) and (222) reflections.

Another common phase detected in all the specimens except in Massa α and in almost all Massa β is cuprite (Cu_2O), which is usually due to the natural alteration of copper. Other alteration phases usually expected for archaeological metal artefacts unearthed after centuries of burial (e.g. chloroargirite, acanthite and nantokite) have not been found. This means that the conservation can be considered good and no relevant corrosion phaenomena are currently present. Lead phase is also missing, although a detection limit of 0.2% must be considered for this metal on INES. Relative phase concentration in our samples are reported in Table 1.

Elemental silver content

The major constituents of the coins alloy are silver and copper phases. Nonetheless, the *d*-spacings measured for the two phases are not those typical of pure elements, i.e 3.6147 Angstrom for copper and 4.0862 Angstrom for silver, and this is the reason why above we specified "copper-rich" phase (α) and "silver-rich" phase (β). The displacement of peaks position in our case is due to non-chemically pure phases and it is the effect of the small solubility interval of the two metals. This phaenomenon is well known for binary alloys and deviations from the theoretical Vegard's law have been studied in depth for different metal alloys[29-32].

Several measurements carried out throughout the years on standard samples have shown the existence of a correlation between lattice parameter and composition for silver-copper phases that can be used to obtain the elemental weight per cent of silver from the phase contents. Being the elemental content the most useful information for numismatists, a calibration curve correlating the lattice parameter variation of α and β with the amount of pure elements can be developed. This was done using data published in literature[33-37], some of them collected in the Pearson's monograph[31,32]. The data used to obtain the calibration curve (Fig. 2 and Supplementary material) concern X-ray diffraction measurements performed on certified samples of known composition, containing exclusively silver and copper, and in general rapidly quenched to avoid diffusion processes. They are referred to the solubility range of copper and silver phases, while those related to metastable phases have been discarded because not useful for this study. The maximum solubility for Cu in Ag and Ag in Cu occurs at the eutectic temperature of 779 °C[38] and the values are, according to the biphasic diagram, respectively of 14.1 at.% for silver and 95.1 at.% for copper[39]. At room temperature this solubility decrease drastically, but a rapid cooling (quenching) guarantee the maintenance of *d*-spacing and composition, being the migration of Ag and Cu at solid state very slow. Concerning pure elements, the lattice parameters used are an average of measurements done by different authors and reported in the Pearson's monograph; in this case, the data refer only to results obtained for measurements executed at room temperature (between 18 and 25°C) and on reference materials with purities > 99.95% for silver and > 99.90% for copper.

It is finally important to notice that the possible presence of other minor or trace element was assumed not to affect the lattice parameter very much. A confirmation is provided by data reported by Pearson[32] for other silver alloys: a silver-gold alloy with 3.3 at.% of gold (a much higher values than that expected in coins) determines a slight *d*-spacing variation of just 0.027%. Hence, the variation of *d*-spacing can be considered exclusively dependent on Ag and Cu content.

[Fig.2]

Four different weighted linear equations (two for each phase, Ag and Cu) have been calculated to fit the data coming from literature (Fig. 2). We used two different calibration curves, one for the silver

and one for the copper phase. For the analysed coins, differences below 0.6 % for silver phase and between 0.4 and 0.8 % for copper phase have been found in comparison to lattice parameters of pure elements. The lattice parameter calculated by means of GSAS was then used, in combination with the curves described above, to calculate the elemental percentage of silver and copper in the α and β phases. These values have to be considered as the actual average occupancy of a silver-rich or copper-rich cell. For this reason it has been necessary a further step of phase refinement in which they have been inserted as the occupancy in place of the unit considered for pure metals. In this way we have correctly taken into account the density variation while evaluating phase composition.

Once *d*-spacing and phase composition have been obtained, the silver content, which is one of the most important information for numismatists, can be easily calculated. We have first of all used the functions to get the ratio of Ag and Cu in the α and β phases. The average atomic weight for these phases has therefore been evaluated, because it changes according to the variation of the two elements. For minor phases, the stoichiometric ratio has been considered instead. Then, for each phase, the number of Ag and Cu atoms have been calculated dividing the phase weight by the average atomic weight and multiplying it for the Avogadro's number. The sum of all the silver atoms can finally be converted into weight (grams) of silver in a coin. The sum of Ag and Cu weight percent is usually very close to 100, except for the cases with considerable quantities of alteration phases. Therefore a normalization has not been done on our samples. Uncertainties for the Ag and Cu elemental content listed in Table 1 come from the propagation of errors on the phases calculation and from the fit used. This method worked very well for these binary alloys because the calculated Ag concentrations for standard materials are compatible (at a significance level of 0.05) with the certified values.

In Fig. 3 are shown results of the elemental composition for the analysed coins. Drachmas are divided according to silver content, typology and suggested chronology[40], even if dating of the first emissions should be revised in the light of new studies[40] and discoveries of the official Massalian drachm[42].

[Fig.3]

The results we obtained allow us to trace very clearly a debasement which affects the Celtic drachm, confirming results obtained on the coins analysed in the previous work[5] but also improving our knowledge on these emissions. The composition of the first Celtic imitations (Massa α) can be compared directly to the fineness content of the original Massalia heavy drachms. The official drachmas of the Greek city have been analysed in a previous work[43] and show a mean silver content of 98% (average on 6 specimens). Our data, along with their co-presence in the Cadenet and La Courtine d'Ollioules (southern France) hoards[44,45], confirm that these first imitations were aligned to the originals, having the same average weight and fineness. This means that they could have circulated together with a ratio 1:1 and that the imitations were not produced with a fraud intent, but for reasons that still have to be deepened. Later drachmas, grouped in the Massa β typology, show again silver concentrations comparable to the Massa α, even if the slight lower weight leave some uncertainties about the ratio exchange of these rare coins.

A second phase of the Celtic coinage is represented by the "naturalistic-lion" and "scorpion-lion" types (III century B.C.), which are often found together in hoards. The quantity of silver detected, 83 wt.% on average, confirm a 1:1 relationship between the two typologies. Nevertheless, we have discovered that some coins (samples 66481; 5590; 5678) classified as belonging to the "scorpion-lion" type do not cluster with others but are spread towards lower values. We have defined in Fig. 3 these coins as a "late scorpion-lion" group. This quite unexpected result is rather interesting, revealing that the "scorpion-lion" group had an internal evolution during the years which lead, at a certain moment, to a

parity with the "wolf-lion" group. Moreover, the three coins with a lower fineness are distinguishable from the others by the use of different dies.

These results confirm the absolutely relative value we should address to stylistic features of ancient coins and that the future for numismatics research lies in the analysis of die links.

Later emissions (II century B.C.), depicting the "lion-wolf", are much more copious. They show a silver average content of 72 wt.% and a close relation with the contemporary Roman *victoriati* can then be supposed, because of a similar fineness content[46]. Metrological relationships with this Roman Republican denomination should anyway be supported by a much careful study and by new analyses, already undergoing.

Elemental analysis through NRCA

Neutron Resonance Capture analysis (NRCA) spectra have been useful especially to check the presence of minor or trace element in the alloy. The main peaks can be assigned to silver (Fig. 4). Peaks belonging to copper are present towards low TOF values (at 109 μs and below). The only trace element detected, in all the specimens, is gold, with three main peaks at 744, 212 and 129 μs. No other elements have been recognized from the analysis of NRCA spectra.

Although a precise quantification of gold content is not possible since the calibration of the NRCA system is still ongoing, an estimate of the order of magnitude has been done using this formula, proposed in a previous work[47]:

$$\rho = \frac{I_{P,Au} \, * \, \sigma_{\gamma,Ag} \, * \, (t_2)^2}{I_{P,Ag} \, * \, \sigma_{\gamma,Au} \, * \, (t_1)^2}$$

where $I_{P,Au}$ and $I_{P,Ag}$ are the peak maxima, $\sigma_{\gamma,Ag}$ and $\sigma_{\gamma,Au}$ are the radiative capture cross-sections of natural Ag and Au respectively and t_1 and t_2 the time positions of the resonance peaks of Ag and Au. The ρ value is the weight ratio between Au and Ag, and the estimates are reported in Table 2. Considering $\rho \approx 0.49$ % we can safely state that such a small quantity of gold could not vary the lattice parameter of the silver cell.

[Table 2]

[Fig.4]

Microstructural properties and working history

In diffraction patterns, the peak shape is related to microstructural properties of the sample, in particular to the presence of residual microstrain, grain domains size and preferred orientation. All these information are important because are the only chance to reconstruct the working history of an object without an invasive metallographic analysis, not applicable on precious archaeological artefacts. When using a GSAS profile function 4, the Gaussian and Lorentzian contributions are defined[24] as:

$$\sigma^2 = \sigma_1^2 d^2 + \sigma_2^2 d^4 + \sigma_S^2 d^6$$

$$\gamma = \gamma_2 d^2 + \gamma_{2e} d^2 + \gamma_S d^3$$

where σ_1^2 is the instrumental broadening, σ_2^2 and γ_2 model the size broadening, σ_S^2 and γ_S represent the strain broadening, γ_{2e} is a negligible term and d is the peak position. All the following parameters for analysed coins are reported in Table 3.

For small crystallites, diffraction lines are no longer Dirac-like, but show widths and shapes depending on the average particle size and shape. For finite size crystallites, the particle size p (in Å) is calculated as follows:

$$p = \frac{DIFC * K}{\gamma_2}$$

where $DIFC$ is a constant for the conversion from TOF into d-spacing for a given diffractometer (~11900 for INES), K is the Sherrer constant (0.8 for a TOF diffractometer) and γ_2 is the Lorentzian parameter linked to the particle size broadening.

The grain dimensions evaluated for the 33 coins analysed in this work (Table 3) appear to be rather small, generally < 60 nm, indicating a very quick cooling of the alloy. Nonetheless, it was slow enough to enable a diffusion of Ag and Cu in the two phases, since the relative concentration of ligands is lower than that expected at the eutectic line. An exception is provided by coin DC 17384, where the grain size is higher than the instrumental upper limit (~100 nm). The Ag grain dimension is constantly higher than that of Cu grains; nevertheless, the lack of grain domain size measurements on reference standards limits our interpretation on these results.

The microstrain broadening can be the consequence of external stresses, mechanical and thermal treatments, crystalline defects or compositional inhomogeneity. The microstrain broadening, Γ_S^2, for a cubic system is defined as

$$\Gamma_S^2 = S_{400} + 3S_{220}$$

where S_{400} and S_{220} are refinable parameters in GSAS. The contribution of S_{220} is negligible, therefore residual strains are directly proportional to S_{400}.

In some samples, microstrain values (Table 3) are higher for the copper rich phase than the silver rich one. Although we still lack studies on this topic, this difference could suggest that a heat treatment was applied prior the minting operation. This treatment, defined as homogenization, consists in heating up the blanks to make them softer for the striking procedure. The difference in microstrain values may be due to the different homogenization temperatures of the two phases. This temperature is slightly lower than the solidus temperature for a given phase. For a copper rich phase, the homogenization occurs in the interval 790/1084°C, while for the silver rich phase is between 790 and 960°C. According to our data, we can hypothesize that the heating was not high enough to erase microstrain, but it was however more effective on the silver rich phase, which requires a lower homogenization temperature. On the other hand, for other samples where S_{400} for α and β phases are substantially similar we should suppose that no heat treatment was applied instead.

A last parameter that has been estimated is the texture index (J), important because related to the working intensity used to strike the coins. While microstrains are linked to elastic deformations, texture is due to plastic ones. This index can be calculated after a preferred orientation correction with a spherical harmonics function, implemented in the GSAS software[49]. This parameter can be considered as an indicator of the order of magnitude of a mechanical stress applied to the material, useful in particular when it is not possible to perform a real texture analysis. On INES, such an analysis would last up to 24 hours for a silver-copper coin and would need to put the coin on a rotating goniometer because of the relatively limited detectors' angular coverage.

Values for the texture index (J) are reported in Table 3. It should be noted that the coins show quite different values, ranging from 1.1 to > 3 both for α and β phases. In general, the value of J varies from 1 (indicating a random isotropic distribution of crystallites) up to infinity, for a sample where crystals have all been oriented in a specific direction. J = 3 indicates a textured sample. Both in Fig. 5a and

Fig. 5b, microstrain and texture index of Ag and Cu phases respectively are reported for all the samples analysed.

[Fig.5(a-b)]

Conclusions

In this work, a selection of Celtic coins from northern Italy has been analysed with the TOF-ND technique. No previous study concerning compositional or microstructural analyses were available: to provide new data for the numismatics research, 33 coins, representative of different emissions, have been studied. The choice of the analytical technique is justified by several reasons. Thanks to the high penetration of neutron, and to a large beam size, average properties of the coins are measured, overcoming surface alterations and inhomogeneity in the blanks. Moreover, ND provides quantitative phase concentration. Weight fractions for major (silver-rich and copper-rich) and minor (mainly cuprite) phases have been calculated trough a Rietveld refinement. Then, a fit has been calculated to relate the lattice parameter and elemental concentration. It is worth noticing that this method can be used in particular for binary Ag-Cu alloys, when no other elements that could modify the lattice parameter are present in relevant quantities (e.g. Au, Pb, Sn). Combining the two information, we indirectly calculated the silver and copper elemental concentration, one of the most important information for numismatists interested in metrology.

Metrological studies are important to determine ratio exchange between different currencies or coins of different periods. For ancient coinages, when no literary sources are available, the only chance is given by the analysis of average weights of a certain emission and by the quantification of precious metal (in this case silver) content. Results obtained in this study show a clear debasement affecting the Celtic drachm, in agreement with data from the coins analysed in the previous work[5] but also improving our knowledge on these emissions. First of all we increased the statistical sample, which is now higher and more significant, especially for the "naturalistic-lion" type. Then, we were able to confirm more certainly the ratio 1:1 between "naturalistic" and "scorpion-lion" types, having the same average silver content. Moreover, analysing coins coming from hoards (and therefore with a more precise chronology) we could understand that the spread values obtained in our previous work[5], are likely due to long-lasting productions, with internal devaluation. Thanks to this work we could find a new sub-group, here defined as "late scorpion-lion", which is stylistically defined and shows a lower silver content, as many of the coins from our previous article. The same remark can be done for the "wolf-lion" type, produced for more than one century and then likely affected by devaluation along the years.

Finally, ND patterns reveal structural properties of materials, allowing to provide useful data for the interpretation of historical production processes. These information have been acquired from the analysis of diffraction pattern. Parameters such as texture index, residual strains and grain dimensions have been extrapolated to reconstruct the metallurgical processes which lead at the production of blanks and, afterwards, the minting. The rather small dimension of crystallites suggests a quick cooling of the alloy, while differences (for some samples) in residual strains between α and β phases reveal a homogenization temperature occurred between 790 and 960°C. We have however to highlight that only few studies concerning the application of diffraction techniques to uncover structural features of ancient coins have been published[50,51], thus our values cannot be compared with other data sets yet.

In conclusion, we can state that information achieved show the importance of TOF-ND for numismatics studies, providing both compositional and microstructural data.

Acknowledgements

References

1. A. Burkhardt and M. Burkhardt, in *I Leponti e la moneta. Atti della giornata di studio (Locarno, 16 novembre 1996)*, eds. E.A. Arslan and R. Carazzetti, Locarno, 2000, pp. 121–136.
2. L. Beck, S. Bosonnet, S. Réveillon, D. Eliot, and F. Pilon, *Nucl. Instrum. Methods Phys. Res. B*, 2004, **226**, 153–162.
3. L. Beck, E. Alloin, C. Berthier, S. Réveillon, and V. Costa, *Nucl. Instrum. Methods Phys. Res. B*, 2008, **266**, 2320–2324.
4. F. J. Ager, A. I. Moreno-Suárez, S. Scrivano, I. Ortega-Feliu, B. Gómez-Tubío, and M. A. Respaldiza, *Nucl. Instrum. Methods Phys. Res. B*, 2013, **306**, 241–244.
5. J. Corsi, B. Maróti, A. Re, Z. Kasztovszky, L. Szentmiklósi, M. Torbágyi, A. Agostino, D. Angelici, and S. Allegretti, *J. Anal. At. Spectrom.*, 2015, **30**, 730–737.
6. W. Kockelmann, E. Pantos, and A. Kirfel, in *Radiation in Art and Archeometry*, Elsevier, 2000, pp. 347–377.
7. W. Kockelmann, S. Siano, L. Bartoli, D. Visser, P. Hallebeek, R. Traum, R. Linke, M. Schreiner, and a. Kirfel, *Appl. Phys. A*, 2006, **83**, 175–182.
8. I. Calliari, C. Canovaro, M. Asolati, A. Saccocci, F. Grazzi, and A. Scherillo, *Appl. Phys. A*, 2013, **113**, 1081–1087.
9. A. Canovaro, I. Calliari, M. Asolati, F. Grazzi, and A. Scherillo, *Appl. Phys. A*, 2013, **113**, 1019–1028.
10. J. Farley, in *Hoards, Hounds and Helmets: A Conquest Period Ritual site at Hallaton, Leicestershire. Leicester Archaeological Monograph 21*, ed. V. Score, 2012, pp. 88–99.
11. I. M. Siouris, S. Katsavounis, and W. Kockelmann, *J. Phys. Conf. Ser.*, 2012, **340**, 012112.
12. A. Kirfel, W. Kockelmann, and P. Yule, *Archaeometry*, 2011, **53**, 930–949.
13. Y. Xie, L. Lutterotti, H. R. Wenk, and F. Kovacs, *J. Mater. Sci.*, 2004, **39**, 3329–3337.
14. W. Kockelmann, A. Kirfel, E. Jansen, R. Linke, M. Schreiner, R. Traum, and R. Denk, in *Numismatics & Technology: questions and answers (Wien, 25-26 April 2003)*, 2003, pp. 113–123.
15. A. Pautasso, *Le monete preromane dell'Italia settentrionale*, Centro di Studi Preistorici e Archeologici di Varese, Varese, 1966.
16. E. A. Arslan, *Sibrium*, 1995, **XXII**, 179–215.
17. M. H. Crawford, *Coinage and money under the Roman Republic: Italy and the Mediterranean economy*, University of California Press, London, 1985, pp. 75-83.
18. G. Gorini, in *Tra protostoria e storia. Studi in onore di Loredana Capuis*, eds. I. Favaretto, E. Ghedini, and G. Gorini, Quasar, Rome, 2011, pp. 281–294.

19. F. Grazzi, M. Celli, S. Siano, and M. Zoppi, *Nuovo Cimento C*, 2007, **30**, 59–65.
20. S. Imberti, W. Kockelmann, M. Celli, F. Grazzi, M. Zoppi, A. Botti, A. Sodo, M. Leo Imperiale, M. de Vries-Melein, D. Visser, and H. Postma, *Meas. Sci. Technol.*, 2008, **19**, 034003.
21. A. Pietropaolo, G. Gorini, G. Festa, E. Reali, F. Grazzi, and E. M. Schooneveld, *Appl. Spectrosc.*, 2010, **64**, 1068–71.
22. F. Grazzi, A. Scherillo, and M. Zoppi, *Rev. Sci. Instrum.*, 2009, **80**, 93704.
23. E. A. Durisi, L. Visca, F. Albertin, R. Brancaccio, J. Corsi, G. Dughera, W. Ferrarese, A. Giovagnoli, N. Grassi, F. Grazzi, A. Lo Giudice, G. Mila, M. Nervo, N. Pastrone, F. Prino, L. Ramello, A. Re, A. Romero, R. Sacchi, F. Salvemini, A. Scherillo, and A. Staiano, *Nucl. Instrum. Methods Phys. Res. A*, 2013, **726**, 31–36.
24. A.C. Larson and R.B. Von Dreele, *General Structure Analysis System (GSAS), Los Alamos National Laboratory Report LAUR*, 1994, **86-748**, 1-224.
25. B.H. Toby, *J. Appl. Crystallogr.*, 2001, **34**, 210-213.
26. Inorganic Crystal Structure Database (ICSD), http://icsd.ill.eu/icsd/
27. H. M. Rietveld, *J. Appl. Crystallogr.*, 1969, **2**, 65–71.
28. *ASM Handbook, Volume 3: Alloy Phase Diagrams*, 1992.
29. F. Grazzi, L. Bartoli, S. Siano, and M. Zoppi, *Anal. Bioanal. Chem.*, 2010, **397**, 2501–11.
30. V.A. Lubarda, *Mech. Mater.*, 2003, **35**, 53–68.
31. W. B. Pearson, *A handbook of lattice spacings and structures of metals and alloys. Volume 2*, Pergamon Press, New York, 1967.
32. W. B. Pearson, *A handbook of lattice spacings and structures of metals and alloys. Volume 1*, Pergamon Press, New York, 1958.
33. E. A. Owen and J. Rogers, *J. Inst. Met.*, 1935, **57**, 257–266.
34. E. Schmid and G. Siebel, *Z. Phys.*, 1933, **85**, 36–55.
35. H. D. Megaw, *Philos. Mag. Ser. 7*, 1932, **14**, 130–142.
36. N. Ageew and G. Sachs, *Z. Phys.*, 1930, **63**, 293–303.
37. N. Ageew, M. Hansen, and G. Sachs, *Z. Phys.*, 1930, **66**, 350–376.
38. H. Moser, J. Otto, and W. Thomas, *Z. Phys.*, 1963, **175**, 327–336.
39. P. R. Subramanian and J. H. Perepezko, *J. Phase Equilib.*, 1993, **14**, 62–75.
40. *La monetazione preromana dell'Italia settentrionale: approvvigionamento del metallo, coniazione, circolazione, Atti dell'Incontro di Studio (Bordighera, 16-17 settembre 1994)*, Istituto Internazionale di Studi Liguri, Bordighera, 1996.
41. M. Py, *Les monnaies préaugustéennes de Lattes et la circulation monétaire protohistorique en Gaule méridionale*, Éditions Aralo, Lattes, 2006.
42. J. Berato, D. Martina-Fieschi, H. Ribot, and J.-M. Theveny, *Préhistoire Anthropologie méditerranéennes*, 1996, **5**, 57–83.
43. J.-N. Barrandon and C. Brenot, *MEFRA*, 1978, **90**, 637–668.
44. C. Brenot, *Bulletin de la Société Nationale des Antiquaires de France*, 1989, 252–257.
45. C. Brenot, in *I Leponti e la moneta. Atti della giornata di studio (Locarno, 16 novembre 1996)*, Locarno, 2000, pp. 11–19.
46. P. Serafin-Petrillo, *Boll. di Numismatica. Supplemento al n° 4*, 1987, pp. 39–49.
47. A. Pietropaolo, G. Festa, F. Grazzi, E. Barzagli, a. Scherillo, E. M. Schooneveld, and F. Civita, *EPL (Europhysics Letters)*, 2011, **95**, 48007p1-48007p4.
48. Database of prompt gamma rays from slow neutron capture for elemental analysis, International Atomic Energy Agency, Vienna, 2007, pp. 54-62.
49. R. B. Von Dreele, *J. Appl. Crystallogr.*, 1997, **30**, 517–525.
50. N. Hadjadj, I. Guillot, and A.-L. Helbert, in *Comprendre les savoir-faire métallurgiques antiques et médiévaux. L'expérimentation archéologique et archéométrique sur la plate-forme expérimentale de Melle*, ed. F. Tereygeol, Errance, Paris, 2013, pp. 111–123.
51. N. Pistofidis, G. Vourlias, T. Dilo, N. Civici, S. Gjongecaj, S. Skolianos, and E. K. Polychroniadis, *Phys. Rev. B: Condens. Matter*, 2010, **405**, 2166–2170.

Coins description				Rietveld refinement results					Calculated results	
Sample code	Provenance	Type	Weight (g)	d-spacing Ag (Å)	d-spacing Cu (Å)	Ag-rich β phase (wt.%)	Cu-rich α phase (wt.%)	Cuprite (wt.%)	Ag (wt.%)	Cu (wt.%)
DC 17378	D.C.	Massa α	3.81	4.0780	-	100.0	-	-	98.7 ± 0.5	1.3 ± 0.1
DC 17379	D.C.	Massa α	3.78	4.0689	-	100.0	-	-	97.3 ± 0.5	2.8 ± 0.1
22653	M.A. Coll.	Massa β	3.43	4.0693	3.6275	96.3	3.7	-	93.9 ± 0.5	6.2 ± 0.1
DC 17380	D.C.	Massa β	3.50	4.0737	-	100.0	-	-	98.0 ± 0.5	2.0 ± 0.1
DC 17382	D.C.	Massa β	3.57	4.0660	-	97.6	2.4	-	94.5 ± 0.5	5.6 ± 0.1
DC 17388	D.C.	Massa β	3.41	4.0626	-	97.5	2.5	-	93.8 ± 0.5	6.2 ± 0.1
DC 17390	D.C.	Massa β	3.62	4.0700	3.6236	85.2	14.0	0.7	83.4 ± 0.5	16.1 ± 0.1
61851	Biandrate	Naturalistic lion	2.28	4.0804	3.6231	82.6	16.8	0.7	82.3 ± 0.5	17.3 ± 0.2
5635	Casale	Naturalistic lion	2.58	4.0803	3.6348	85.0	12.9	2.1	85.0 ± 0.5	13.6 ± 0.1
5524	Casale	Naturalistic lion	3.14	4.0732	3.6240	80.6	18.9	0.5	79.5 ± 0.5	20.2 ± 0.1
87502	Serra Riccò	Naturalistic lion	2.67	4.0720	3.6250	84.0	14.8	1.2	82.6 ± 0.5	16.6 ± 0.2
5716	Casale	Naturalistic lion	3.25	4.0700	3.6272	91.5	8.2	0.3	89.4 ± 0.5	10.4 ± 0.1
66500	Serra Riccò	Scorpion lion	2.94	4.0848	3.6238	83.4	16.3	0.4	83.7 ± 0.5	16.1 ± 0.2
66503	Serra Riccò	Scorpion lion	3.05	4.0762	3.6236	83.8	15.3	0.9	82.9 ± 0.5	16.5 ± 0.2
5712	Casale	Scorpion lion	2.71	4.0755	3.6251	83.4	15.6	0.9	82.5 ± 0.5	16.8 ± 0.2
5551	Casale	Scorpion lion	3.00	4.0793	3.6213	84.9	14.2	0.9	84.3 ± 0.5	15.1 ± 0.1
DC 17384	D.C.	Scorpion lion	2.75	4.0708	3.6312	84.0	14.5	1.5	82.6 ± 0.5	16.3 ± 0.1
87509	Serra Riccò	Scorpion lion	2.95	4.0793	3.6212	81.9	17.3	0.8	81.4 ± 0.5	18.1 ± 0.2
66493	Serra Riccò	Scorpion lion	2.66	4.0773	3.6217	84.2	13.8	1.9	83.3 ± 0.5	15.3 ± 0.1
66489	Serra Riccò	Scorpion lion	3.19	4.0617	3.6309	82.2	17.3	0.5	79.7 ± 0.5	19.9 ± 0.2
5644	Casale	Scorpion lion	3.27	4.0802	3.6237	80.6	18.8	0.6	80.4 ± 0.5	19.2 ± 0.2
5571	Casale	Scorpion lion	3.04	4.0763	3.6231	86.6	11.7	1.6	85.6 ± 0.5	13.2 ± 0.1
66481	Biandrate	Late scorpion lion	2.73	4.0738	3.6327	70.7	28.5	0.8	70.7 ± 0.5	28.7 ± 0.2
5590	Casale	Late scorpion lion	2.80	4.0775	3.6228	74.8	24.7	0.5	74.4 ± 0.5	25.3 ± 0.2
5678	Casale	Late scorpion lion	2.97	4.0756	3.6248	74.3	24.4	1.4	73.8 ± 0.5	25.4 ± 0.2
61822	Biandrate	Wolf lion	2.62	4.0809	3.6264	72.0	27.2	0.8	72.3 ± 0.5	27.1 ± 0.2
61843	Biandrate	Wolf lion	2.78	4.0745	3.6228	72.4	26.6	1.0	71.7 ± 0.5	27.6 ± 0.2
66478	Biandrate	Wolf lion	2.75	4.0709	3.6236	71.3	27.7	0.9	70.3 ± 0.5	29.0 ± 0.2
61828	Biandrate	Wolf lion	2.02	4.0795	3.6222	69.1	30.5	0.4	69.0 ± 0.5	30.7 ± 0.2
66483	Biandrate	Wolf lion	3.34	4.0702	3.6271	69.0	30.4	0.6	68.3 ± 0.5	31.3 ± 0.2
66480	Biandrate	Wolf lion	2.41	4.0755	3.6237	84.0	15.3	0.7	83.0 ± 0.5	16.5 ± 0.1
66485	Biandrate	Wolf lion	2.73	4.0745	3.6235	70.6	28.5	1.0	70.0 ± 0.5	29.4 ± 0.2
61845	Biandrate	Wolf lion	2.77	4.0689	3.6271	75.8	24.1	0.1	74.6 ± 0.5	25.4 ± 0.2
Standard 1, MBH (Ag wt.%: 94.40 ± 0.04)				4.0647	3.6327	98.6	1.4	-	95.3 ± 0.5	4.7 ± 0.1
Standard 2, MBH (Ag wt.%: 87.60 ± 0.06)				4.0646	3.6216	90.7	9.3	-	87.8 ± 0.5	12.3 ± 0.2
Reference material, Goodfellow (Ag wt.%: 72)				4.0717	3.6195	75.3	24.7	-	73.9 ± 0.5	26.1 ± 0.4

Table 1. Data and results concerning the composition of the 33 drachmas and 3 standard materials analysed with TOF-ND. Standard deviation for the weight is ± 0.01 g. Uncertainty for the d-spacing in of the order of ± 0.0001 Å. Standard deviation for the phase concentration is of the order of ± 0.1 - 0.5 wt.%. D.C. stands for "Dotazione Corona", indicating specimens coming from the royal collection of King Carlo Alberto in Turin (Medagliere Reale). M.A. Coll. stands for the collection of the Museo di Antichità in Torino.

Peak intensity Ag (a.u.)	Peak intensity Au (a.u.)	Radiative capture cross section ^{107}Ag and ^{109}Ag (b)	Radiative capture cross section ^{197}Au (b)	Time position Ag (μs)	Time position Au (μs)	ρ Au (At. %)	Radiative capture cross section reference
0.68	0.58	58	108	724	745	0.49	[48]

Table 2. Data used to estimate the gold content in coin 66485.

Sample code	Provenance	Type	Microstrain (S400) Ag	Microstrain (S400) Cu	Grain size Ag (nm)	Grain size Cu (nm)	Texture index Ag (J)	Texture index Cu (J)
DC 17378	D.C.	Massa α	2.11 ± 0.14	-	43 ± 2	-	1.58	-
DC 17379	D.C.	Massa α	2.32 ± 0.12	-	42 ± 2	-	1.15	-
22653	M.A. Coll.	Massa β	3.31 ±0.29	-	29 ± 2	-	1.52	-
DC 17380	D.C.	Massa β	2.34 ± 0.19	-	30 ± 1	-	1.36	-
DC 17382	D.C.	Massa β	1.65 ± 0.11	-	60 ± 4	-	1.18	-
DC 17388	D.C.	Massa β	7.47 ± 0.40	-	35 ± 3	-	4.03	-
DC 17390	D.C.	Massa β	4.46 ± 0.31		29 ± 2	-	1.51	-
61851	Biandrate	Naturalistic lion	2.97 ± 0.25	3.63 ± 0.36	31 ± 2	49 ± 5	1.60	1.60
5635	Casale	Naturalistic lion	4.26 ± 0.32	7.71 ± 0.81	24 ± 1	50 ± 9	1.10	1.06
5524	Casale	Naturalistic lion	2.13 ± 0.17	2.24 ± 0.19	30 ± 1	51 ± 3	1.11	1.14
87502	Serra Riccò	Naturalistic lion	4.42 ± 0.35	3.12 ± 0.40	35 ± 3	43 ± 4	1.98	2.00
5716	Casale	Naturalistic lion	2.28 ± 0.18	1.57 ± 0.40	27 ± 1	44 ± 6	1.11	1.07
66500	Serra Riccò	Scorpion lion	4.13 ± 0.30	4.29 ± 0.37	29 ± 2	44 ± 4	1.24	1.28
66503	Serra Riccò	Scorpion lion	2.89 ± 0.18	2.57 ± 0.24	35 ± 2	46 ± 3	3.36	3.45
5712	Casale	Scorpion lion	3.12 ± 0.22	3.32 ± 0.30	31 ± 1	52 ± 4	1.26	1.42
5551	Casale	Scorpion lion	3.37 ± 0.24	3.41 ± 0.32	29 ± 1	46 ± 4	1.13	1.22
DC 17384	D.C.	Scorpion lion	0.81 ± 0.22	1.51 ± 0.53	> 100	> 100	1.49	1.50
87509	Serra Riccò	Scorpion lion	3.79 ± 0.25	4.35 ± 0.37	36 ± 2	45 ± 4	2.92	3.57
66493	Serra Riccò	Scorpion lion	2.89 ± 0.23	3.23 ± 0.38	31 ± 2	49 ± 6	1.77	1.86
66489	Serra Riccò	Scorpion lion	7.11 ± 0.34	4.36 ± 0.30	32 ± 2	51 ± 4	2.76	2.50
5644	Casale	Scorpion lion	2.46 ± 0.87	4.45 ± 0.33	27 ± 1	39 ± 3	1.16	1.16
5571	Casale	Scorpion lion	2.48 ± 0.19	2.37 ± 0.32	32 ± 2	42 ± 3	1.08	1.12
66481	Biandrate	Late scorpion lion	3.90 ± 0.43	3.99 ± 0.27	22 ± 1	43 ± 3	1.90	1.57
5590	Casale	Late scorpion lion	2.28 ± 0.20	3.38 ± 0.21	32 ± 2	47 ± 2	1.13	1.22
5678	Casale	Late scorpion lion	2.94 ± 0.25	3.70 ± 0.24	29 ± 2	45 ± 3	1.07	1.19
61822	Biandrate	Wolf lion	2.30 ± 0.22	3.97 ± 0.77	35 ± 2	52 ± 4	1.40	1.67
61843	Biandrate	Wolf lion	2.57 ± 0.26	3.13 ± 0.22	32 ± 2	48 ± 3	1.39	1.45
66478	Biandrate	Wolf lion	1.95 ± 0.17	2.77 ± 0.16	37 ± 2	48 ± 2	1.43	1.81
61828	Biandrate	Wolf lion	2.24 ± 0.25	3.95 ± 0.21	29 ± 2	52 ± 3	1.06	1.15
66483	Biandrate	Wolf lion	3.49 ± 0.28	4.03 ± 0.57	36 ± 2	53 ± 3	2.00	2.43
66480	Biandrate	Wolf lion	3.09 ± 0.22	4.18 ± 0.35	28 ± 1	43 ± 3	1.71	1.99
66485	Biandrate	Wolf lion	1.49 ± 0.17	2.70 ± 0.15	30 ± 1	52 ± 2	1.22	1.30
61845	Biandrate	Wolf lion	2.71 ± 0.22	2.97 ± 0.18	29 ± 1	54 ± 3	2.63	2.66

Table 3. Results concerning structural parameters extracted from diffraction patterns of the 33 drachmas analysed with TOF-ND.

Figures

Fig.1. The heavy drachm of Massalia (a) and imitations. Massa α type (b), Massa β type (c), "naturalistic-lion" type (d), "scorpion-lion" type (e), "wolf-lion" type (f). All the coins bear the same figures, but with different stylistic features. Reference bars: 1 cm each.
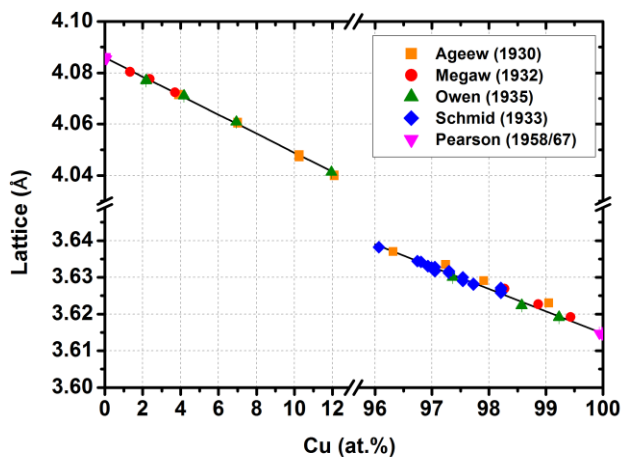

Fig. 2. Correlation between lattice parameter and Cu concentration. Plotted data on the left refer to the solubility range of Ag-rich phase, while those on the right refer to Cu-rich phase. Data are taken from different studies (see the Supplementary Material for a detailed listing).
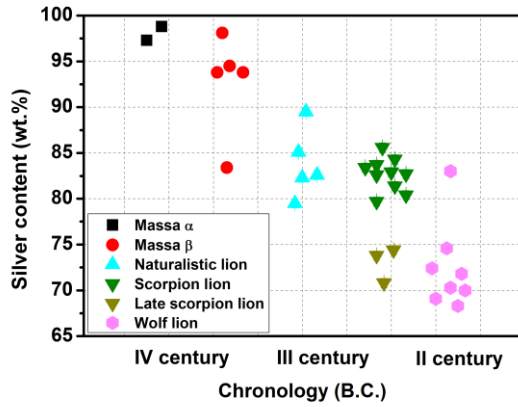
Fig. 3. Drachmas grouped according to silver content and typology. A debasement is apparent among different emissions.
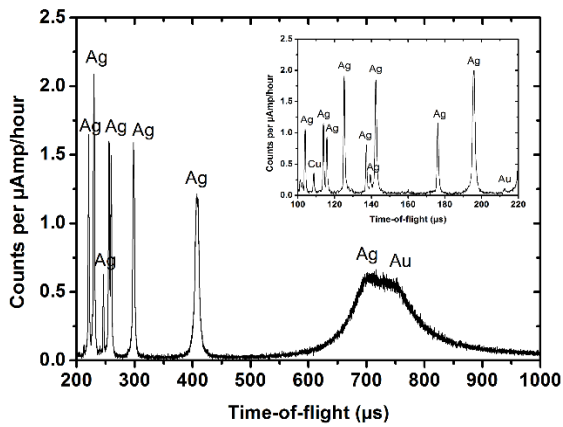

Fig. 4. Neutron Resonance Capture Analysis (NRCA) spectra of the coin 66485, with major peaks labelled.
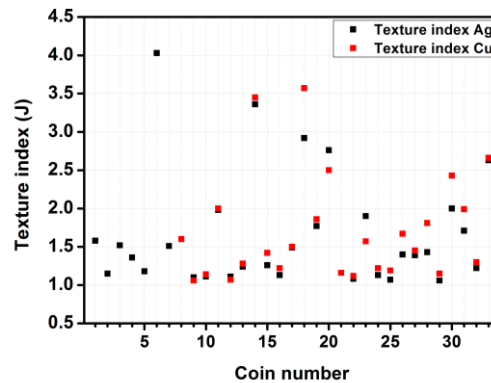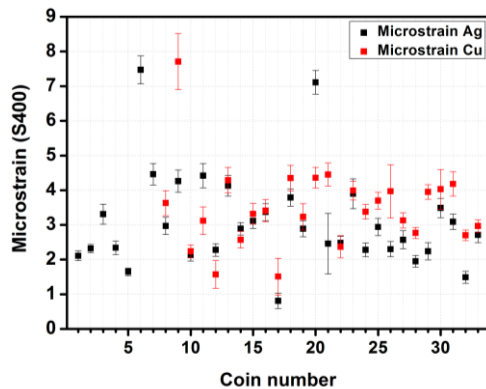

Fig. 5 (a-b). Microstrain broadening and texture index for the analysed coins. The coin number follows the row order of Table 3.